A-14 CRACK EXTENSION AND PROPAGATION UNDER PLANE STRESS

A. R. Rosenfield[†], P. K. Dai[††] and G. T. Hahn[†]

ABSTRACT

Experiments are described that reveal the three-dimensional character of the plastic zone in front of notches and cracks in plates of an Fe-3Si steel and a plain carbon steel. These define the plane-stress regime as a function of applied stress and plate thickness. They also provide a rationale for the DM (Dugdale-Muskhelishvili) model as a tentative elastic-plastic solution of a crack under plane stress. Refinements that offer a way of taking work hardening and rate-sensitive plastic deformation into account are described. In this way, unnotched tensile properties — the stress-strain curve and reduction in area — are used to calculate plastic-zone size, crack-tip displacements and strains, the crack-extension stress, and the fracture toughness, in accord with experiments. Finally, the approach is extended to ductile crack propagation and used to calculate the crack speed and the stress, strain, and strain rates imposed on material in advance of a moving crack.

INTRODUCTION

Treatments of crack extension in metals based on the solutions of Inglis[1] and Griffith[2] fail because they regard the metal as completely elastic. The modified-elastic solutions of Orowan[3] and Irwin[4] are more successful. These make adjustments for local plastic deformation, but they do not describe stress and strain in the region adjacent to the crack tip. Further progress demands elastic-plastic solutions that can describe in detail what happens in the plastic zone, and these will make it possible to predict crack extension from the unnotched mechanical properties. Inroads into the elastic-plastic problem have been made by Allen and Southwell[5], and others[6-9], and further progress can be expected. Yet, at this writing,

[†] Metal Science Group
Battelle Memorial Institute
Columbus, Ohio, 43201, U.S.A.
[††] Air Force Materials Laboratory
Wright-Patterson Air Force Base, Ohio, 45433, U.S.A.

there are no rigorous solutions that define the local stress and strain for a crack in tension under either plane strain or plane stress; the solution for the intermediate case is not even in sight.

This paper explores two alternate methods of attacking the plane-stress problem: (1) experimental measurements and (2) a special elastic-plastic solution which compromises generality and rigor for simplicity. The experiments reveal the character of the plastic zone in front of cracks and notches in an Fe-3Si steel and a plain carbon steel plate. In this way, they offer a rationale for the DM (Dugdale-Muskhelishvili) model.(10,11) It has already been shown(10,12) that this model makes reasonably good predictions of plastic-zone size and crack-tip displacement under plane-stress conditions. In this paper, a refined version of the DM model, capable of taking work hardening and rate-sensitive yielding into account, is described. Plastic-zone size, crack-tip displacements and strains, the crack-extension stress, and K_c† are calculated in this way from unnotched properties. The calculations are also extended to the case of a propagating ductile crack, and they define the crack speed as well as the stresses, strains, and strain rates generated in advance of the crack. Where possible, calculations are compared with experiment, and the resulting correlations support the usefulness of the DM model.

OBSERVATIONS OF PLASTIC ZONES

Procedure and Materials

This section deals with the three-dimensional character of the plastic zone in front of a crack and how it changes with nominal stress and plate thickness. The experiments follow along lines previously reported(12), but are more complete and systematic. The plastic zones were generated by edge notches in rectangular coupons†† of an Fe-3Si steel (Si, 3.31%; C, 0.04%) and a plain carbon steel (Project Steel E(13): C, 0.22%; Mn, 0.36%). These coupons, derived from stress-relieved plates (1 hour at 475°C) of warm-rolled Fe-3Si steel††† and hot-rolled Steel E, were machined in thicknesses ranging from 0.453 inch to 0.017 inch.

Two types of notches were studied: (1) a 0.25-inch-deep by 0.006-inch-wide saw cut (root radius ~0.003 inch), and (2) a 0.25-inch-deep fatigue crack††††. After machining and notching (and fatiguing), the coupons were recrystallized††††† to anneal out traces of deformation introduced during machining and fatiguing. One set of Fe-3Si steel coupons was annealed at

† Linear elastic fracture-toughness parameter.

†† Eight inches long by 2.5 inch wide, with a centrally located 4-inch-long gage section.

††† Reduced 50 percent at 300°C.

†††† Grown from 0.12-inch-long by 0.006-inch-wide saw cuts by cycling the coupons in tension between 4,000 and 38,000 psi.

††††† Fe-3Si: 800°C for 1 hour; Steel E: 900°C for 1 hour.

1200°C, a high temperature intended to coarsen the grain size and eliminate discontinuous yielding. As a final step, the surfaces of the test coupons were electropolished with the Morris reagent(14).

The notched coupons were then slowly loaded to various stress levels in a tensile-testing machine; the peak load was maintained for 4 minutes and then gradually released. Stress levels are reported either as T, the net section stress, or as T/Y, the ratio of net section stress to yield stress. As the next step, residual strains normal to the plate surface were detected and recorded with the aid of an interference microscope. Following this, Fe-3Si steel samples were aged 20 minutes at 150°C to decorate the dislocations.

Plastically deformed regions on the surface of Fe-3Si steel were revealed by etch-pitting electrolytically in Morris reagent. The coupons were then sectioned, repolished, and etched to reveal the plastic zone in the interior. The plain carbon steel could not be etched. In its case, plastic zones are revealed on the surface by virtue of slight surface tilts which accompany the plastic deformation.

True-stress/true-strain curves of the Fe-3Si and plain carbon steels are reproduced in Figure 1a, and other data are given in Table 1. Figure 1 shows graphically the stress-strain formulations, described in Table 1, that serve as inputs to the computer calculations and are discussed later. A complete list of symbols and their definitions appears in Appendix A.

Experimental Results

Figure 2 shows the plastic zones revealed on the surface of Fe-3Si steel plates of different thicknesses and their development with increasing applied stress. The interpretation given previously(12) is that there are two different types of zones – one associated with plane strain, and the other with plane stress conditions:

1. Plane Strain. At low stress levels, two yielded regions fan out in directions roughly normal to the plane of the crack (the ±y-direction, Figure 2g; see Figures 2c, 2f, 2g, and 2h); at this stage, ρ_H, the extent of the zone in the y-direction (Figure 2g) is smaller than the plate thickness, there is little strain normal to the plate surface, and the zone is effectively invisible on the unetched coupons. Etched interior sections, parallel to the plate surface, display nearly the same zone shape, and this zone has the character of flow around hypothetical plastic hinges qualitatively in accord with Jacobs'(6) plane-strain calculations and the experiments of Green and Hundy.(15)

2. Plane Stress. At high stress levels, large tapering wedges project forward in front of the crack (the x-direction, Figure 2g; see Figures 2a and 2b, 2d and 2e, and 2i) from the ends of the two fans. On the surface, the two wedges are always separated by a distance corresponding to the plate thickness (see Figures 2b, 2e, and 2i). Etching interior sections parallel to the plate surface reveals that

the two wedges merge into a single wedge on the midsection, as shown in Figure 3. Normal sections (see Figure 4) confirm that the wedges are in reality wedgelike regions inclined at 45 degrees to the tensile axis where shear has occurred through the thickness direction. At this stage there is, in fact, noticeable strain through the thickness direction in the form of a depression (dimple) on the surface.

More detailed studies, now in progress, reveal 45-degree-shear near the plate surface and in the interior, even when the plastic zone is much smaller than the plate thickness. It is, therefore, more correct to regard Fe-3Si-steel plastic zones as composites: partly hinge, and partly inclined wedge. At low stress levels, particularly for short cracks and thick plates, the hinge component predominates, while for suitable combinations of high stress, long crack, and thin section, the inclined wedges make the major contribution.

The plastic zones observed on the electropolished surfaces of the plain carbon steel (Figure 5) are also interpreted as inclined wedges. Here, although a number of wedge-shaped zones are nucleated†, the growth of only one is favored, and this wedge is longer than the corresponding wedges in the Fe-3Si steel (compare Figures 2 and 5 and note the difference in magnification). Since the wedges appear above the crack centerline on one side of the plate, and below on the opposite surface, they undoubtedly represent a single 45-degree-inclined wedge.

It can be seen in Figures 6a and 6b that notch acuity has little effect on either size or the shape of the inclined wedge component — that is, the zone character under plane-stress conditions††. Also shown in Figures 6c and 6d (these correspond to Curves 1.1 and 1.2 in Figure 1a) is the effect of the yield drop. Comparison reveals that the difference between a material with a yield drop and one without is less than experimental error. This evidence refutes the suggestion of Durelli et al[16], and Dixon and Visser[17] that the wedge-shaped plastic zone is due to the yield drop, as such. It also opens to question the view of McClintock and Irwin[18] that the effect is mainly the result of low work-hardening rate. As a contrast to the Fe-3Si steel contour, Figure 6e shows the profile for plain carbon steel. Comparison with the visual observations (for example, Figure 3) reveals that the zone represents a tilt on the surface, as suggested previously.

The transition from a dominant hinge to a dominant wedge (for example, from plane strain to plane stress) is gradual and therefore difficult to define. It seems likely that the hinge will dominate so long as 45-degree-shear is constrained; that is, so long as the inclined wedges are contained by elastic material and do not penetrate to the plate surfaces. Such penetration will not have occurred so long as the portion of the hinge visible on the surface extends a distance $\rho_H < t/2$ on either side of the crack (see

† These can probably be interpreted as Lüders' bands.

†† There is a marked effect of notch acuity on the distribution of strain within the hinge component, particularly close to the root radius. This will be described in more detail in a future publication.

Figure 2g; t is the plate thickness). This serves as an approximate criterion for plane strain. The contribution of the wedges probably begins to exceed that of the hinge when the wedge length $\rho > 4t$ (see Figure 2i). This is merely a rough estimate and serves as a tentative criterion for plane stress. In both instances, ρ_H and ρ increase with increasing applied stress. Consequently, the transition from plane strain to plane stress will occur at higher stresses in thicker sections. This is shown qualitatively in Figures 2 and 5 and more quantitatively in Figure 7. For example, the 0.017-inch-thick coupon (Figure 2a) already displays 45-degree-shear prominently when the nominal stress is 40 percent of the yield stress; whereas in the 0.200-inch-thick coupon, stresses in excess of 90 percent of yield are required (Figure 2i).

From the evidence presented, it is possible to construct stylized three-dimensional pictures of the plastic zone under plane-stress conditions As shown in Figure 8, the zones displayed by the plain carbon and Fe-3Si steels are basically similar. They consist of either a long, single, 45-degree inclined wedge, or two long 45-degree inclined wedges intersecting at 90 degrees. Figures 8d and 8c show, schematically, that the wedges are attached to the hinge portion; but the exact pattern of deformation in the region where the hinge and wedge merge is not yet clear.

THE DM MODEL

The Simple Model

In the light of the preceding section, Dugdale's model of a crack with wedge-shaped plastic zones takes on special significance. The model, illustrated in Figures 9a and 9b, consists of a crack of length 2c in an infinite plate. When the plate is subjected to a nominal stress, T, plastic zones of length ρ are generated at either end. Together, the zones and the crack are assumed to have the shape of the stressed elastic slit shown in Figure 9b. The material within the plastic zone is then replaced by an "equivalent" distribution of internal tension, S(x), acting on the slit interface — equivalent in the sense that it simulates the support that was derived from the yielded material. This final step transforms the elastic-plastic problem into a purely elastic one that can be treated by the Muskhelishvili conformal mapping procedures.[11]†

The DM model possesses a zone lying in the plane of the crack, as opposed to the 45-degree-inclined wedge(s) that dominate real plane-stress zones (see Figure 8c). The model also possesses a special wedge shape, effectively a Tresca yield criterion, and a material that undergoes no further elastic deformation after yielding. These assumptions may not be overly restrictive. For example, the distinction between a straight and an inclined wedge is minimized as ρ becomes larger than t, and vanishes as $t \to 0$. The DM model is useful — to the extent the various assumptions are

† Barenblatt[19] has adopted a similar approach to treat the finite cohesive strength of completely brittle materials.

applicable or not crippling — because it transforms the complex three-dimensional plastic region into a much simpler one-dimensional zone.

Dugdale[10] considered the simple case where S(x) is a uniform distribution equivalent to Y, the yield stress of the material (see Figure 9c). For this case, the following can be formulated explicitly in terms of c, T, and Y:

(a) The elastic stress gradient[12], $\sigma(x)$ for $y = 0$

(b) The plastic-zone size[10], ρ

(c) The displacement gradient[20], $v(x)$ for $c < x \leq \rho$

(d) The crack-tip displacement[20], $v_c \equiv v_{(x = c)}$.

The relevant equations are summarized in Table 2.

So far, albeit limited, experimental tests of these equations have been encouraging. Dugdale's[10] zone-size measurements performed on mild steel are described very well by Equation 4. Hahn and Rosenfield[12] found that zone size and crack-tip displacement values measured for Fe-3Si steel are in reasonable accord with Equations 4 and 5a. For example, the criterion for plane stress, $\rho > 4t$, can be formulated via Equation 4 as

$$\frac{c}{t} > 4\left(\sec\frac{\pi T}{2Y} - 1\right)^{-1} \quad , \tag{14}$$

and this is consistent with the experimental measurements given in Figure 7. The criterion for plane strain, $\rho_H < t/2$, can be formulated on the basis of Tetelman's observation that $\rho_H \approx \rho/2$, and is

$$\frac{c}{t} < \left(\sec\frac{\pi T}{2Y} - 1\right)^{-1} \quad , \tag{15}$$

and this is also in reasonable accord with the measurement. Equations 14 and 15 indicate that the zone character is determined by the dimensionless parameter, c/t, and this gives the results of Figure 7, obtained solely by changing t, greater generality.

At the same time, some discrepancies between theory and experiment have been noted[10,12]. At the higher stresses, Dugdale's measured ρ values and those for Fe-3Si steel (see Figure 7 for $c/t < 2$, where some of the half-filled points lie in the plane-stress region) are consistently smaller than predicted. This is related to work hardening; the increase with strain of $\overline{\sigma}$, the flow stress in the plastic zone, means that the value of S becomes larger than Y. At the same time, the load-bearing cross section within the plastic zone diminishes as a consequence of constant-volume plastic deformation, and this ultimately leads to local necking and a reduction in S. The net effect is an S(x) of the form shown in Figure 9d (rather than the simpler form of Figure 9c adopted by Dugdale), and this is treated in the next section.

Modified DM Model

Work hardening and constant-volume deformation influence two things: (1) the distribution of internal tension, S(x), and (2) the y distribution of strain in the plastic zone, which is shown in Figure B-1 and discussed more fully in Appendix B. This distribution fixes the relation between v and $\overline{\varepsilon}$,

$$\overline{\varepsilon} = f(v) \quad , \tag{16}$$

where v is the displacement at a given distance, x, along the abscissa, $c \leq x \leq (c + \rho)$, and $\overline{\varepsilon}$ is the maximum true-plastic strain at the same distance. At present, the form of Equation 16 must be derived from experiment, and the simple model presented in Appendix B offers an approximate way of formulating the distribution in terms of the measurable quantity, d, the width of the plastic zone (see Figure 5f),

$$\overline{\varepsilon} = \ell n\left(\frac{d + 2v}{d - 2v}\right) \approx \frac{4v}{d} \quad . \tag{16a}$$

To simplify matters further, the ratio d/t is assumed to remain constant. The idea of relating strain and displacement in terms of a fixed distance, d, has been advanced by Goodier and Field[20].

The same model also describes t′, the minimum-section thickness at a given distance, x, along the abscissa, $c \leq x \leq (c + \rho)$, and this connects the value of S with $\overline{\sigma}$,

$$S = \overline{\sigma}\left(\frac{t'}{t}\right) = \overline{\sigma}\exp\left(-\overline{\varepsilon}\right) \quad , \tag{17}$$

and (via Appendix B),

$$S = \overline{\sigma}\left(\frac{d - 2v}{d + 2v}\right) \quad . \tag{17a}$$

The flow strength and work-hardening rate of material within the zone is expressed by the true-stress/true-strain characteristics,

$$\overline{\sigma} = f(\overline{\varepsilon}) \quad . \tag{18}$$

Some of the calculations that will be described exploit the following $\overline{\sigma} - \overline{\varepsilon}$ equation,

$$\overline{\sigma} = \frac{Y}{B^n}\left[\overline{\varepsilon} + B\right]^n \quad , \tag{18a}$$

where Y, B, and n are material constants. This is equivalent at all but small strains to the more usual power law, $\overline{\sigma} = K\overline{\varepsilon}^n$, but has the advantage that $\overline{\sigma}\ (\overline{\varepsilon} = 0) = Y$.

Together, Equations 5, 16, 17, and 18, or the more specific forms used here (Equations 16a, 17a, and 18a), offer a first estimate of internal-stress

distribution, S(x). The resulting function is approximated by a stepwise distribution, as shown in Figure 9e. Then, via Equations 7 to 13 in Table 2 (these are the analogies to Equations 1 to 6 for the case of a stepwise internal-stress distribution) and particularly Equation 12, successive approximations of S(x) can be obtained. This reiterative process leads to the correct form of S(x) and appropriate values of ρ, $\sigma(x)$, $v(x)$, as well as $\bar{\varepsilon}(x)$ and $\bar{\varepsilon}_c$. The procedure, while prohibitive by hand, is easily managed on a digital computer. The flow diagram of a computer program is given in Appendix C. It is programmed for an IBM-7094 Fortran II system located at Wright-Patterson Air Force Base, Ohio.

Plastic-Zone Calculations

Results of computer calculations exploiting the modified DM model and results derived from the simpler form are presented in Figures 10 and 11. The values in Figure 10 were calculated for Curve 1.4 (Figure 1b, Table 1) intended to match a 4330M steel. Figure 10a compares the distribution of internal tension; Figure 10b shows the elastic stress gradient and true-stress values within the plastic zone; Figure 10c gives corresponding values of the plastic strain gradient. It should be noted that the strain values quoted at the various relative distances, x/c, are the true strains at the minimum section (see Equation B-2, Appendix B); the value of the crack-tip strain, $\bar{\varepsilon}_{(x = c)} \equiv \bar{\varepsilon}_c$ (see Figure 10c), is the maximum strain generated within the DM zone. Figures 10b and 10c illustrate that the crack not only concentrates the stress, but is a potent "strain concentrator" as well. Figure 11a shows that the plane-stress zone size measurements of Dugdale ($\rho/t \geq 4$), while in accord with the simple theory, agree even better with the predictions of the modified DM model. Figure 11b shows similar results for Fe-3Si steel. This is good evidence that the systematic deviation from the simple model can be attributed to work hardening rather than a strain-rate effect.[10] The correlation also lends some confidence to the other calculations which have not been tested.

Figures 12a and 12b summarize plastic-zone calculations for the hypothetical "high-strength" and "conventional" steels in Figure 1c (Curves 1.7, 1.8, and 1.9; Table 1). These are intended to show, in a general but quantitative way, the influence of strength level and work-hardening rate on zone size and crack-tip strain. Figure 12a illustrates that the strength level has little effect on zone size when the comparison is made at the same relative nominal-stress level, T/Y†. This follows from Equation 4a, valid at low stress. On the other hand, Figure 12b shows that strength level can have a significant effect on $\bar{\varepsilon}_c$, even at comparable T/Y values; the crack produces larger strains within the higher strength material†. This has important implications for fracture and is a consequence, first, of the factor Y/E which appears in Equation 5a and, secondly, of Equation B-2, for example,

$$\bar{\varepsilon}_c \sim \frac{v_c}{t} \sim \left(\frac{c}{t}\right)\left(\frac{Y}{E}\right)\left(\frac{T}{Y}\right)^2 \quad . \tag{19}$$

† Assuming n and d/t are unchanged.

Thus, the crack-tip strain also depends on plate thickness. The value of the work-hardening exponent has a modest effect on ρ and $\bar{\varepsilon}_c$†, via its effect on the S(x) distribution. The quantity n may actually have a larger influence than is at first apparent, because it probably modifies the zone width, d.

APPLICATION OF THE MODIFIED DM MODEL TO CRACK EXTENSION

In the preceding section, the DM formalism was used to treat the growth of a wedgelike plastic zone. The model can also deal with the growth of the crack itself if the cracking is by ductile shear or fibrous fracture. These mechanisms usually involve large strains locally, and the plane-stress criterion, $\rho > 4t$, can be satisfied. The analysis can take advantage of the fact that states of stress and strain generated within the wedgelike DM zone are similar to those produced in the neck of an unnotched plate or sheet coupon††. Indeed, fractures in unnotched tensile bars of copper involve thin zones of heavily deformed material[22]. The cracks form within the zones at a terminal stage of hole coalescence[22], irrespective of whether the plate is notched or unnotched, and this stage is conveniently identified by the strain at fracture††† In this way, a critical strain criterion for fracture of material in the region adjacent to the crack tip (the most heavily strained region) can be adopted,

$$\bar{\varepsilon}_c \geq \bar{\varepsilon}^* \quad , \tag{20}$$

where $\bar{\varepsilon}^*$ is the ductility of the unnotched material in terms of true strain as calculated, for example from RA, the reduction in area [$\bar{\varepsilon}^* = -\ell n(1\text{-RA})$]. Equation 20 is also the criterion for crack instability (crack extension), because the strain imposed on material ahead of the extending crack continues to increase, $\frac{d\bar{\varepsilon}_c}{dc} > 0$ (Equation 5a of Table 2 and Equation B-2), while its capacity for strain, $\bar{\varepsilon}^*$, remains constant. The quantity $T^* \equiv T_{(\bar{\varepsilon}_c = \bar{\varepsilon}^*)}$ is the nominal crack extension or fracture stress of the cracked plate, and $K_c = T^*\sqrt{\pi c}$, where K_c is the linear elastic fracture-toughness parameter. Values of T^* and K_c can be computed with the same equations and program described in the last section. For the given conditions:

† At constant Y and d/t.

†† The large triaxial stress component generated when the crack is under plane strain is absent under plane stress (by definition). The smaller triaxial stress component associated with the neck is present in both cases. The conditions in the notched coupon are also similar to those in a round test bar, since the influence of the biaxial stress component (normal to tensile axis and in the plane of the plate) on the stress and strain at fracture is probably small.

††† Provided the rates of straining are comparable, the fracture condition is represented by a single point on the $\bar{\sigma} - \bar{\varepsilon}$ curve. Either the true stress or the true strain at fracture identifies this point; but strain is more convenient.

(a) Geometry, c and t

(b) Flow properties, $\bar{\sigma} = f(\bar{\varepsilon})$ (for example, Y, B, and n, Table 1) and d

(c) Ductility, $\bar{\varepsilon}^*$ (reduction in area),

and an assumed value of T, the quantity $\bar{\varepsilon}_c$ is calculated and compared with $\bar{\varepsilon}^*$. T is then appropriately adjusted and the procedure repeated until $\bar{\varepsilon}_c \to \bar{\varepsilon}^*$; concurrently, $T \to T^*$. Two exceptions to this procedure are noted in the footnote below.†

Calculations of this kind were tailored for a 4330M steel and a 2219-T87 aluminum alloy. The crack-extension stress of these materials had previously been measured over a range of crack lengths[23] (see Figure 13). Fractures were of the ductile shear variety. The $\bar{\sigma} - \bar{\varepsilon}$ curves could be constructed from published data, and RA values are reported in the literature (see Figure 1b, Curves 1.4 and 1.5, and Table 1). Only the values of d, the zone width, have not been measured; the values quoted in Table 1 are rough estimates based on observations of similar materials.

As shown in Figure 13, both the general trend and the absolute values of T^* and K_c calculated in this way are in good accord with the experimental values. It is particularly significant that the modified DM theory predicts the decrease in K_c evident when $\frac{T^*}{Y} > 0.8$, an effect that is beyond the reach of linear elastic-fracture mechanics[23]. Figure 13a shows curves calculated for two widely differing values of d/t, and this gives some indication of the uncertainty introduced by incomplete knowledge of this parameter.

The influence of strength level, work-hardening rate, and ductility on T^* and K_c was calculated†† for the two hypothetical steels of Figure 1c, and the results are summarized in Figures 12c and 12d. All three material parameters play a significant role in determining fracture strength. Figure 12c illustrates that there is not a one-to-one correlation between strength level and the fracture stress; the relative fracture stress T^*/Y at 30,000 psi is higher than at the 300,000-psi strength level (see Figure 12c). This effect, which assumes importance for all "high-strength" materials, has as its origin the role of Y/E in Equation 5b. The net result, shown more clearly in Figure 14a, is that the ΔT^* associated with a fixed ΔY decreases as the strength level is raised when $\bar{\varepsilon}^*$, n, and d are constant. In practice, some ductility and work-hardening capacity are usually sacrificed to obtain higher strengths, with the result (as shown by the shaded band in Figure 14a) that the fracture stress becomes relatively insensitive to yield strengths above 200,000 psi. This means that the benefits (in terms of increased fracture toughness) of strength-level increases above 200,000 psi are likely to be marginal if they are accompanied by decreased ductility and work-hardening rate.

The kind of "trade-offs" that may be encountered for a 300,000-psi steel (see Curve 1.7, Figure 1c, and Table 1) can be anticipated by the calculations of the type summarized in Figure 14b. For example, a 33 percent or 100,000-psi increase in Y, accompanied by a 20 percent loss in both the RA and n†, would net only a modest 9 percent of 17,000-psi gain in fracture stress. Calculations of this kind offer useful guidelines to the metallurgical origins of fracture toughness and the potential value of specific material improvements.

APPLICATION OF THE MODIFIED DM MODEL TO CRACK PROPAGATION

The balance of forces between the elastic matrix and the plastic zone for stresses below T^* is a form of static equilibrium. When the stress exceeds T^* and the crack begins to accelerate, the system enters a state of dynamic equilibrium controlled by the dynamic yield characteristics, provided the plastic response of the material is rate sensitive††. The main difference is that the distribution of internal tension now reflects the flow stress consistent with both the local strain and the local strain rate. In this way, the rate with which the material strains to the critical value, $\bar{\varepsilon}^*$, determines the crack speed. When the effective crack length grows continuously, the equilibrium is constantly displaced and the crack accelerates. In special cases, the effective crack length is limited by a finite dimension of the structure, and a steady state may be attained. This mechanism does not consider inertia effects and is only valid for crack speeds and accelerations substantially below the limits set by the dynamic analysis of Mott[24] and Roberts and Wells[25].†††

† Exception 1: Failure by yielding at $T = Y$. In some cases, $\bar{\varepsilon}_c < \bar{\varepsilon}^*$ even when $T \geq Y$. Failure is then assumed to occur by gross yielding and $T^* \equiv Y$. An alternative approach, not used here, is to consider the plate at a uniform strain, $\bar{\varepsilon}_T \equiv \bar{\varepsilon}(\bar{\sigma} = T)$. A crack of length c is now cut, and the plastic zone is the region where $\bar{\varepsilon} > \bar{\varepsilon}_T$. The origin of the $\bar{\sigma} - \bar{\varepsilon}$ curve is shifted so that $\bar{\varepsilon}_T$ corresponds to $\bar{\varepsilon} = 0$, and $Y \equiv \bar{\sigma}(\bar{\varepsilon} = \bar{\varepsilon}_T)$. The critical strain is now $\bar{\varepsilon}^{**} \equiv \bar{\varepsilon}^* - \bar{\varepsilon}_T$, and the model can be applied as before.

Exception 2: Failure by yielding at $T < Y$. In some instances, $\bar{\varepsilon}_c < \bar{\varepsilon}^*$, but the ratio ρ/c becomes very large. The failure is then a form of plastic instability, and $T^* \equiv T_{\rho \to \infty}$.

†† For constant, d/t.

† This corresponds to a change from RA = 30% ($\bar{\varepsilon}^* = 0.35$) to RA = 24% ($\bar{\varepsilon}^* = 0.27$), and from n = 0.05 to n = 0.04.

†† If the resistance to plastic deformation increases with increasing strain rate.

††† The velocity calculated by Mott[24] and Roberts and Wells[25], relevant for the rate-insensitive material,

$$u = 0.38\, u_s \sqrt{1 - \frac{c^*}{c}} \quad ,$$

can be regarded as an upper limit (u_s is the longitudinal wave velocity, and c^* is the crack length at instability).

When the inertia effect can be ignored, the problem can be treated with the modified DM model†. The only additional requirement is a description of the true stress in terms of strain and strain rate,

$$\sigma = f(\bar{\varepsilon}, \dot{\bar{\varepsilon}}) \quad . \tag{21}$$

A specific example of Equation 21, derived from dislocation-dynamics considerations[26], is useful for this purpose:

$$\bar{\sigma} = A_1 \bar{\varepsilon}^n + (\dot{\bar{\varepsilon}})^{\frac{1}{m}} \left(A_2 + A_3 \bar{\varepsilon}\right)^{-\frac{1}{m}} \quad . \tag{22}$$

It can describe an upper and a lower yield point (see Curves 1.10, Figure 1d), different degrees of rate sensitivity, and its constants can have theoretical significance. The equation is used to perform the steady-state calculations described in the following paragraphs. These are of a preliminary nature, and are intended merely to demonstrate the application of the DM model to the dynamic case.

The crack speed and the stress, strain, and strain-rate gradients in front of the crack were calculated for a propagating ductile-shear fracture. The case considered is a crack traveling alont the x-axis at steady state and at constant velocity†† for a fixed nominal stress, T > T*, under the following conditions:

(i) Geometry. $\frac{c}{t} = 200$.

(ii) Dynamic flow characteristics. Relation III, Table 1; the constants were selected to approximate the response of mild steel in the strain-rate range 10^{-1} to 10^{+3} per second (see Curves 1.10, Figure 1d, and Table 1). There is evidence that the constants used slightly overestimate rate sensitivity of steel when $\dot{\bar{\varepsilon}} < 10^{-1}$ sec^{-1} and seriously underestimate it when $\dot{\bar{\varepsilon}} > 10^{3}$ sec^{-1}, and this must be taken into account in future calculations. Relation III (Table 1) is reasonable for a mild steel with Y = 40,000 psi when measured at $\dot{\bar{\varepsilon}} = 10^{-4}$ sec^{-1}.

The expression for d [footnote (c) in Table 1] is derived from actual measurements of a shear fracture in a mild steel involving a fast-moving crack.

(iii) Ductility. The value $\bar{\varepsilon}^* = 0.33$ (RA = 28%) was derived from the shear fracture mentioned above; the value $\bar{\varepsilon}^* = 0.40$ (RA = 33%) was for purposes of comparison.

The numerical procedure begins with a trial stress distribution and a trial velocity, u_o. First, approximations of the quantities $\bar{\varepsilon}$, $\frac{d\bar{\varepsilon}}{dx}$, $\dot{\bar{\varepsilon}}$, $\bar{\sigma}$,

† Goodier and Field[20] have applied the DM model to the dynamic problem, but their calculations do not take rate-sensitive yielding into account.

†† Essentially a moving axis analysis, since the effective crack length must remain constant.

and S(x) are obtained†, and the process is repeated until the solution converges. Then $\bar{\varepsilon}_c$ is compared with $\bar{\varepsilon}^*$, the trial value u_o is adjusted accordingly, and the process of evaluating $\bar{\varepsilon}_c$ is repeated. In this way, as $\bar{\varepsilon}_c \to \bar{\varepsilon}^*$, $u_o \to u$, and stress, strain, and strain-rate gradients consistent with the velocity are determined. The singularity of strain gradient at x = a is avoided in the computation by smoothing out the strain-distribution curve near the elastic-plastic boundary. This process is justified because the cusp is very localized in nature, and in reality one does not expect such a cusp to occur.

Figures 15 and 16 are examples of the results of dynamic calculations. Figure 15 shows the relation between nominal stress and crack velocity. The velocity appears to be exceedingly sensitive to T for speeds below 500 feet per second. Higher speeds generate strain rates in excess of 10^3 sec^{-1} in the plastic zone (see Figure 16c), and the steel probably enters the regime of greater rate sensitivity. For this reason, the crack velocity is likely to be less sensitive, and this is shown qualitatively by the dashed portions of the curves in Figure 15. The calculations also indicate that ductility can have a significant influence on crack speed.

Stress, strain, and strain-rate gradients are reproduced for two crack speeds in Figure 16. The stress gradients reveal peaks at the leading edges of the plastic zone which are manifestations of the yield point. These are in doubt, and are shown in dashed lines for two reasons: (1) the computations are inaccurate in this region, and (2) there is some question whether the deficiency of mobile dislocations, that accounts for the yield point in an annealed material, can exist at an elastic-plastic interface[26]. The 600-ft/sec velocity was chosen as an example because shear fractures traveling at speeds from 500-800 feet per second are encountered in practice[27]. Figure 16c indicates that the behavior of such fast-moving fractures is controlled, at least in part, by the material's response to strain rates from 10^2 to 10^4 sec^{-1}. This range is relatively unexplored — a factor limiting crack-speed calculations of this kind. The high rates also mean that present calculations probably underestimate the stresses in front of the 600-ft/sec crack (Figure 16a).

The present calculations tend to confirm the results obtained earlier by Hahn, Reid, and Gilbert[28] with a much cruder model: (1) stresses of the order of 100,000 psi are attained ahead of fast-moving cracks in steel, and (2) the plastic zone is smaller at higher speeds (Figure 16a). The high stresses plus the triaxial component associated with a shorter and less-wedgelike zone will favor cleavage fracture. It is anticipated that further calculations of this kind will prove useful for describing the ductile-to-brittle transition behavior of steel.

† $\dot{\bar{\varepsilon}} \equiv \frac{d\bar{\varepsilon}}{d\tau} \sim \frac{d\bar{\varepsilon}}{dx} u_o$; $\bar{\sigma}$ is given by Equation 22.

DISCUSSION

The DM analysis is versatile, and there is evidence supporting its relevance in specific cases. The real questions are its general applicability and the precision this approach offers — and these are points that warrant discussion and more experimentation. Clearly, real plastic zones deviate from the ideal DM wedge. How seriously do these and other assumptions affect the predictions of the model?

Long wedgelike zones have now been observed under plane-stress conditions(Equation 14)in silicon steel, in plain carbon steel[10,16, 17,29-31], in high-strength steel[32], in cold-rolled copper[29,33], and in stainless steel[35]. The wide range of configurations employed in these investigations tends to confirm our observation that the appearance of the DM zone does not depend critically on notch geometry. Consequently, this type of zone is not an isolated phenomenon. It seems likely that all of these are wedges inclined at 45 degrees to the tensile axis. This deviation does not appear to be serious in view of the agreements between theory and experiment.

In some cases, wedges also intersect the plate surface at 45 degrees to the x-axis (refer to Figure 9). These "side bands" have been observed by Dixon and Visser[17] and Durelli et al[16] in steel, and by Druyvesteyn et al[33] in hard-rolled copper sheet, but not by the present investigators. In general, they are found in conjunction with the more usual zones discussed above. The type of deformation contributed by side bands and their influence on the local strain distribution is not clear.

The plastic zones observed by Bateman et al[30] on the surfaces of cracked aluminum alloys are not elongated wedges but circular in character. At first glance, they may seem a departure from the conceptual picture developed here; but this is not the case. Bateman's tests involve combinations of stress, crack length, and thickness that place the zone in the lower portion of the transition region between plane stress and plane strain (Figure 7). Contour maps of the circular zones are comparable to the one obtained for the zone shown in Figure 2h. This does not prove that all plane-stress zones are wedgelike, but again shows that both the stress level and the crack length-to-thickness ratio must be taken into account in comparisons.

The hinge component close to the tip of the crack represents another deviation from the theoretical DM zone. There is some evidence that the behavior of this portion of the plastic zone is similar to the wedge. Bateman's measurements[30] and those of Tetelman[22] indicate ρ_H, the extent of predominantly hinge zones, obeys the same functional relation as ρ and is about one-half the value predicted for plane stress. Furthermore, the equations describing zone size and displacements for plane-stress tension[10] and both plane-[9] and anti-plane-shear[19] are nearly identical. In spite of this, the hinge complicates crack extension. Within the influence of the hinge, stable crack growth ("pop-in") is possible along lines formulated by McClintock[34]. This comes about because the deformed regions extend out to large y-distances. As the crack extends, these regions are left behind and new zones take their place at the crack tip. A crack with this history of local yielding, extension,

and more local yielding (as opposed to a virgin crack of the same length) generates smaller strains. Consequently $\delta\varepsilon_c/\delta c$ can be negative, and the condition $\overline{\varepsilon}_c > \overline{\varepsilon}^*$ may not be maintained. Stable crack growth within the hinge in the early stages of loading can be incidental to the unstable growth mechanism fostered by the wedge-shaped zones; but it will modify the stress-strain distribution, and may cause departures from the DM model. The plastic-zone history will also tend to stabilize the shear crack growing within the wedge zone. In this case, plastic deformation is largely confined to the region immediately in front of the crack; the effect is thus likely to be smaller, and the condition $\frac{\delta\overline{\varepsilon}_c}{\delta c} > 0$ may still be fulfilled. Shear crack growth implies that the crack is in the plane of a 45-degree-inclined wedge, and this presents a problem since the starting crack is usually pictured normal to the tension axis. The crack must therefore reorient itself, and this probably occurs in the region influenced by the hinge component. The existence of this reorientation stage need not radically alter the criterion for crack extension employed in this paper, but probably modifies it in some way. For these reasons, agreements cited here between crack-extension experiments and the DM theory should be regarded with caution.

Still another important deviation is the fact that the zone width, d, and displacement, v, do not coincide (see Figure 9a). While this does not invalidate zone-size or zone-displacement predictions, it does preclude the possibility of calculating strain directly. This is a crucial point, because the distribution of strain in the y-direction is a prerequisite for calculating ductile fracture and for implementing the work-hardening and strain-rate corrections. The concept of a strain distribution involving a constant width, d, exploited here, is convenient but oversimplified; both d and the character of the distribution may change with stress and distance from the crack tip. Certainly, a general solution of the configuration of the neck in an unnotched sheet or plate would offer useful insights — but this problem apparently has not been worked out. Further experiments characterizing the strain distribution under load may offer the possibility of correlating this with the shape of the stress-strain curve.

CONCLUSIONS

Under plane-stress conditions, localized plastic zones at notches and cracks in an Fe-3Si steel and a plain carbon steel are dominated by long 45-degree-inclined wedge-shaped regions. These wedges resemble the plastic zones attending Dugdale's plane-stress model (DM model) of a crack in an elastic-plastic material. The mathematical treatment of the "simple" DM model offers reasonable descriptions of zone sizes and displacements in real materials. A "modified" form of the same model can deal with work-hardening and rate-sensitive plastic deformation. In this way, the stress, strain, and strain-rate gradients, the crack-extension stress, effects of work hardening and ductility, and the speed of propagating cracks can be calculated.

Comparisons of zone-size and fracture-stress calculations with experiments show that predictions of the modified DM model can be reasonably accurate. Furthermore, it is a powerful tool in the hands of the alloy developer, since it shows quantitatively how much strength level, ductility, and the work-hardening rate contribute to fracture toughness. Preliminary calculations offer promise for describing the propagation of ductile cracks and the transition from ductile-to-brittle fracture. These calculations are limited by the lack of good stress-strain data at strain rates approximating those at the tip of a fast-running crack.

ACKNOWLEDGMENTS

The authors are indebted to the Ship Structure Committee for sponsoring the experimental part of this study, and to the Air Force Materials Laboratory of the Research and Technology Division for supporting the analytical portion. Studies for the American Gas Association provided the foundation and set the stage for the developments described here. Expert technical assistance was provided by Messrs. P. Mincer and R. Stephenson and by Lt. G. C. Smith. This is gratefully acknowledged along with the discussions and encouragement of R. I. Jaffee, G. K. Manning, W. J. Trapp, and F. C. McClintock. Invaluable assistance was provided by the staff of the Digital Computer Division at Wright-Patterson Air Force Base.

REFERENCES

(1) C. E. Inglis, Trans. Instn. Nav. Archit., London, England, 55 (1913), 219.

(2) A. A. Griffith, Phil. Trans. Roy. Soc., A221 (1920), 163.

(3) E. Orowan, Reports Prog. Phys., 12 (1949), 185.

(4) G. R. Irwin, J. Appl. Mech., 24 (1957), 361.

(5) D. N. de G. Allen and R. V. Southwell, Phil. Trans., A242 (1950), 379.

(6) J. A. Jacobs, Phil. Mag., 41 (1950), 349.

(7) L. D. Stimpson and D. M. Eaton, Tech. Rep. ARL24, California Institute of Technology, 1961.

(8) J. A. H. Hult and F. A. McClintock, 9th Int. Cong. Appl. Mech., 8 (1957), 51.

(9) B. A. Bilby, A. H. Cottrell, and K. H. Swinden, Proc. Roy. Soc., A272 (1963), 304.

(10) D. S. Dugdale, J. Mech. Phys. Solids, 8 (1960), 100.

(11) N. I. Muskhelishvili, Some Basic Problems of the Mathematical Theory of Elasticity, Noordhoff, Gronigen, Holland (1953), p 340.

(12) G. T. Hahn and A. R. Rosenfield, Acta Met., 13 (1965), 293.

(13) G. T. Hahn, B. L. Averbach, and M. Cohen, J. Iron Steel Inst., 200 (1962), 634.

(14) C. E. Morris, Metal Prog., 56 (1949), 696.

(15) A. P. Green and B. B. Hundy, J. Mech. Phys. Solids, 4 (1956), 128.

(16) A. J. Durelli, A. Kobayashi, and K. Hofer, Exptl. Mech., 1 [9], (1961), 1.

(17) J. R. Dixon and W. Visser, Proc. Intnl Symp. Photoelasticity (edited by Frocht), Pergamon Press, Oxford, England (1963), p 231.

(18) F. A. McClintoch and G. R. Irwin, ASTM Symposium on Crack Toughness Testing and Applications (June 1964).

(19) G. I. Barenblatt, Prikl. Mat. i. Mekh., 24 (1960), 316.

(20) J. N. Goodier and F. A. Field, Fracture of Solids (edited by Drucker and Gilman), Interscience Publishers, New York (1963), p 103.

(21) A. S. Tetelman, Acta Met., 12 (1964), 993.

(22) H. C. Rogers, Trans. Amer. Inst. Min. (Metall.) Engrs., 218 (1960), 498.

(23) ASTM Committee on Fracture Testing of High Strength Materials, Materials Research & Standards, 4 (1964), 107.

(24) N. F. Mott, Engineering, 165 (1948), 16.

(25) D. K. Roberts and A. A. Wells, Engineering, 178 (1954), 820.

(26) G. T. Hahn, Acta Met., 10 (1962), 727.

(27) A. R. Duffy and G. M. McClure, Oil & Gas J., 61 [38] (1963), 12.

(28) G. T. Hahn, A. Gilbert, and C. N. Reid, J. Iron Steel Inst., 200 (1964), 677.

(29) H. W. Liu, Appl. Matls Res., 2 (1964), 229.

(30) D. A. Bateman, F. J. Bradshaw, and D. P. Rooke, Tech. Note CPM 63, Royal Aircraft Establishment (March 1964).

(31) J. R. Dixon and J. S. Strannigan, J. Mech. Eng. Sci., 6 (1964), 132.

(32) J. L. McCall, Battelle-Columbus Laboratories; private communication, 1964.

(33) M. J. Druyvesteyn, F. T. Klosterman, J. Roos, P. M. vanDijk, P. Los, and S. Radelaar, J. Mech. Phys. Solids, 12 (1964), 219.

(34) F. A. McClintock, J. Appl. Mech., 25 (1958), 582.

(35) R. G. Forman, Tech. Doc. Rep., AFFDL-TR-65-146, (Wright Patterson AFB, Ohio) (1965)

APPENDIX A: NOTATION

a = Crack plus plastic-zone length

A_1, A_2, A_3, B = Parameters in the stress-strain equations

c = Crack length

c_i = Point in plastic zone where step change in internal tension is applied

d = Plastic-zone width

E = Young's modulus

K_c = Fracture toughness

m = Strain-rate sensitivity, $d \log \bar{\sigma}/d \log \dot{\epsilon}$

n = Strain-hardening exponent

RA = Reduction in area

S = Internal tension

T = External applied stress

T^* = Crack-extension stress

t = Specimen thickness

t' = Minimum specimen thickness at crack tip

u = Crack velocity

u_o = Trial crack velocity

v = Displacement

v_c = Crack-tip displacement

x = Distance from center of crack in direction of crack

x_j = Discrete value of x used in computation

y = Coordinate axis normal to crack plane

Y = Yield stress

α = arc cosh x/a ($x \geq a$)

β = arc cos c/a

$\bar{\epsilon}$ = True strain

$\bar{\epsilon}^*$ = True strain at fracture

$\dot{\bar{\epsilon}}$ = Plastic-strain rate

$\bar{\epsilon}_c$ = True strain at crack tip

$\bar{\epsilon}_L$ = Lüders' strain

ν = Poisson's ratio

θ = arc cos x/a ($x \leq a$)

θ_j = arc cos x_j/a ($x_j \leq a$)

ρ = Plastic-zone size (plane stress)

ρ_H = Plastic-zone size (plane strain)

σ = Stress

$\bar{\sigma}$ = True stress

τ = Time

APPENDIX B: THE DISPLACEMENT-STRAIN RELATION

A simplified model of the plastic-zone strain distribution is shown in Figure B-1. Figure B-1a shows the cross section of a plate, of thickness t, at the distance $c \leq x \leq \rho$; the line AA identifies the plane of the crack. The deforming region is arbitrarily confined to a height, d. It is also assumed that strains in the x-direction can be neglected. Under stress, this region extends to a length (d + 2v) at constant volume, and the plate consequently necks as shown schematically in Figure B-1b. Necking tends to localize deformation, but the neck cannot become too small or plastic deformation will be constrained. Although, to account for constant volume deformation the plastic-zone width grows larger than d, for the majority of cases treated here, this growth is small, d >> 2v. Thus the width of the plastic zone remains roughly constant. The neck is approximated by the double trapezoid of Figure B-1c. Since the deformation involves no volume change, the area of the trapezoid, d·t, is constant, and this fixes the minimum section t',

$$t' = t\left(\frac{d - 2v}{d + 2v}\right) \quad . \tag{B-1}$$

The maximum true-strain, $\bar{\epsilon}$, is the strain corresponding to the minimum section,

$$\bar{\epsilon} = \ln\left(\frac{t}{t'}\right) = \ln\left(\frac{d + 2v}{d - 2v}\right) \approx \frac{4v}{d} \quad . \tag{B-2}$$

The tension, S, supported at x and $\bar{\sigma}$, the true-stress acting at the minimum section can also be related,

$$S = \bar{\sigma}\left(\frac{t'}{t}\right) = \bar{\sigma}\left(\frac{d - 2v}{d + 2v}\right) = \bar{\sigma} \exp(-\bar{\epsilon}) \quad . \tag{B-3}$$

In this way, values of $\bar{\epsilon}$, $\bar{\sigma}$, and S can be calculated if v, d, $\bar{\sigma} = f(\bar{\epsilon})$ are known.

TABLE 1. PARAMETERS DESCRIBING STRESS-STRAIN BEHAVIOR OF MATERIALS OF FIGURE 1

Material	Curve No.	True-Stress/ True-Stress Relation[a]	Tensile Properties			Deformation Parameters				
			E (10^6 psi)	Y (10^3 psi)	RA (%)	A_1 (10^3 psi)	B	n	$\bar{\epsilon}_L$	d/t
Fe-3Si Steel	(1.1)	II	30.0	62.4	70	128.8	--	0.165	0.012	1.0
	(1.2)	I	30.0	54.0	--	--	--	0.16	0.0	--
Mild Steel	(1.3)	II	30.0	35.0	63	98.0	--	0.249	0.01	--
4330M Steel	(1.4)	I	30.0	189.0	45	--	0.0063	0.100	--	0.5, 1.0
2219-T87 Al	(1.5)	I	11.0	59.0	30	--	0.0054	0.075	--	1.0
Dugdale's Steel	(1.6)	II	30.0	28.0	63	87.0	--	0.25	0.015	0.5
Hypothetical	(1.7)	I	30.0	300.0	--	--	0.005	0.05	--	1.0
	(1.8)	I	30.0	30.0	--	--	0.005	0.2	--	1.0
	(1.9)	I	30.0	30.0	--	--	0.005	0.05	--	1.0
Mild Steel	(1.10)	III	30.0	40.0[b]	28, 33	98.0	--	0.431	--	(c)

(a) Relation I: $\bar{\sigma} = \frac{Y}{B^n}(\bar{\epsilon} + B)^n$

Relation II: $\bar{\sigma} = Y$ for $\bar{\epsilon} \leq \bar{\epsilon}_L$

$\bar{\sigma} = A_1 \bar{\epsilon}^n$ for $\bar{\epsilon} \geq \bar{\epsilon}_L$

Relation III: $\bar{\sigma} = A_1 \bar{\epsilon}^n + \left(\frac{\dot{\bar{\epsilon}}}{4.02 \times 10^{-63} + 5.39 \times 10^{-58}\,\bar{\epsilon}}\right)^{1/13}$

(b) Static Yield Stress

(c) For this steel, Equation B-2 was replaced by

$$\epsilon_c^* = \ln\left(1 + \frac{v}{0.117t + .01}\right)$$

TABLE 2. IMPORTANT EQUATIONS OF THE DM MODEL

The Simple Model

(a) Normalized Coordinates:

$$\cos\beta = \frac{c}{c+\rho}, \quad \cos\theta = \frac{x}{c+\rho} \tag{1}$$

$$\cosh\alpha = \frac{x}{c+\rho}; \quad x \geq (c+\rho) \tag{2}$$

(b) To Remove Stress Singularity at Tip of Plastic Zone:

$$\beta = \frac{\pi T}{2Y} \tag{3}$$

(c) Plastic-Zone Size:

$$\frac{\rho}{c} = \sec\beta - 1 \tag{4}$$

$$\frac{\rho}{c} = \frac{\pi^2}{8}\left(\frac{T}{Y}\right)^2; \quad \left(\frac{T}{Y}\right) \leq 0.6 \tag{4a}$$

(d) Crack-Tip Displacement:

$$V(x) = \frac{2a}{\pi}\frac{Y}{E}\left[\cos\theta \ln\frac{\sin(\beta-\theta)}{\sin(\beta+\theta)} + \cos\beta \ln\frac{(\sin\beta+\sin\theta)}{(\sin\beta-\sin\theta)}\right] \tag{5}$$

$$v_c = \frac{4cY}{\pi E}\ln\sec\beta \tag{5a}$$

$$v_c = \frac{\pi cY}{2E}\left(\frac{T}{Y}\right)^2; \quad \left(\frac{T}{Y}\right) \leq 0.6 \tag{5b}$$

(e) Stress in Elastic Region ($x \geq a$, $y = 0$):

$$\sigma_y = T\left[1 - \frac{1}{2\beta}\delta_a(\beta)\right] \tag{6}$$

$$\delta_a(\beta) = 2\arctan\left(\frac{\sin 2\beta}{\cos 2\beta - e^{-2\alpha}}\right) \tag{6a}$$

The Work-Hardening Model

(a) Normalized Coordinates:

$$\cos\beta_i = \frac{c_i}{c+\rho} \quad (c_1 \equiv c) \tag{7}$$

$$\cosh\alpha = \frac{x}{c+\rho}; \quad x \geq (c+\rho) \tag{8}$$

$$\cos\theta_j = \frac{x_j}{c+\rho}; \quad x_j \leq (c+\rho) \tag{9}$$

(b) To Remove Stress Singularity at Tip of Plastic Zone:

$$\frac{\pi T}{2} = \sum_{i=1}^{n} \beta_i \left(S_i - S_{(i-1)}\right); \quad S_0 \equiv 0 \tag{10}$$

(c) Plastic-Zone Size:

$$\frac{\rho}{c} = \sec\beta_1 - 1 \tag{11}$$

(d) Crack-Tip Displacement:

$$v(x_j) = \frac{2a}{\pi E}\sum_{\substack{i=1 \\ i\neq j}}^{n}\left(S_i - S_{(i-1)}\right)\left[\cos\theta_j \ln\frac{[\sin(\beta_i-\theta_j)]}{[\sin(\beta_i+\theta_j)]} + \cos\beta_i \ln\frac{(\sin\beta_i+\sin\theta_j)}{(\sin\beta_i-\sin\theta_j)}\right] + 4c_j\frac{[S_j - S_{(j-1)}]}{\pi E}\ln\sec\beta_j \tag{12}$$

$$v_c = v(x_j)_{x_j = c} \tag{12a}$$

(e) Stress in Elastic Region ($x \geq a$, $y = 0$):

$$\sigma_y = T - \frac{1}{\pi}\sum_{i=1}^{n}\left(S_i - S_{(i-1)}\right)\delta_a(\beta_i) \tag{13}$$

$$\delta_a(\beta_i) = 2\arctan\left(\frac{\sin 2\beta_i}{\cos 2\beta_i - e^{-2\alpha}}\right) \tag{13a}$$

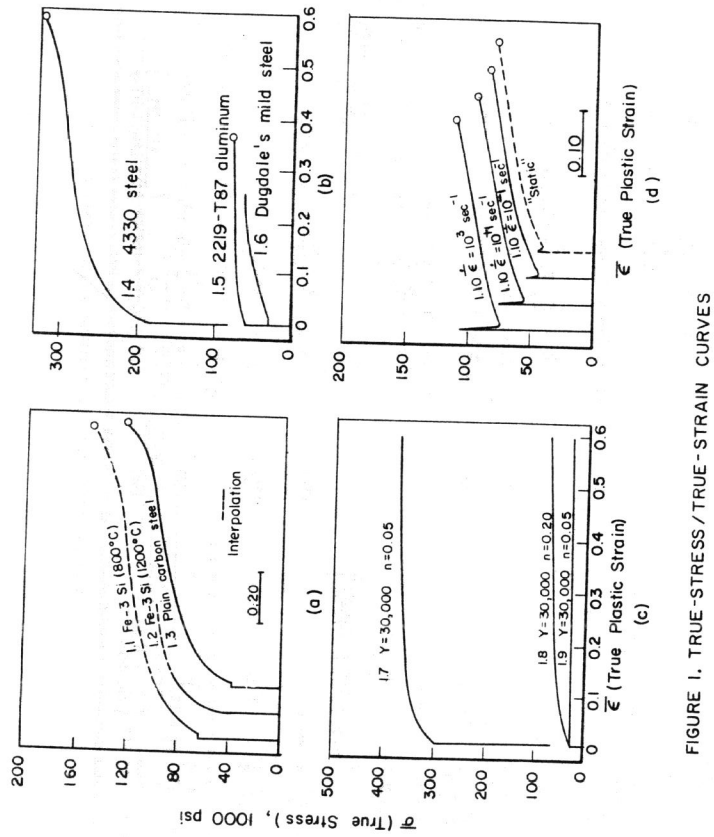

FIGURE 1. TRUE-STRESS/TRUE-STRAIN CURVES

(a) Curves for experimental materials; (b, c, & d) curves correspond to $\bar{\sigma}$-$\bar{\epsilon}$ equations given in Table 1.

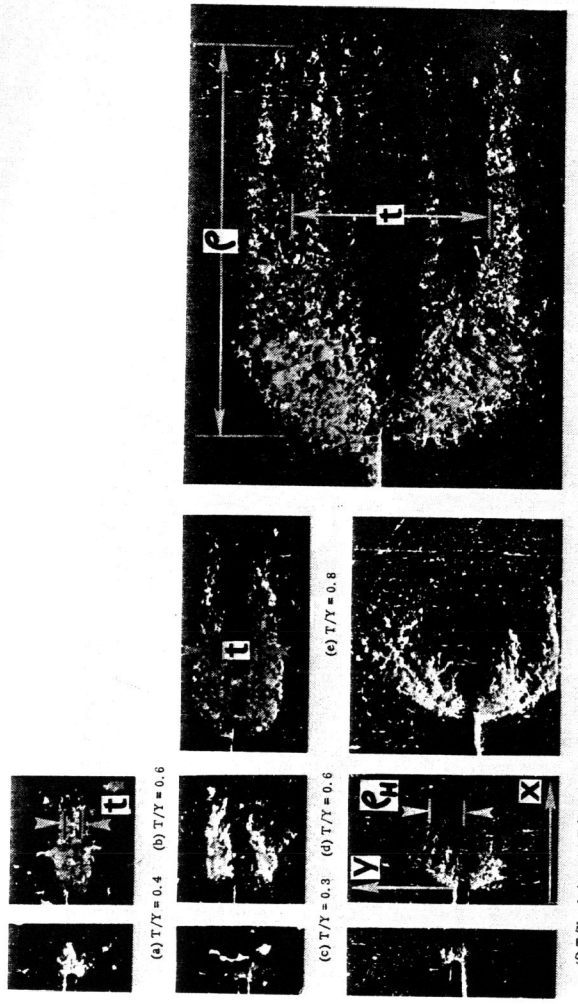

FIGURE 2. INFLUENCE OF NOMINAL STRESS AND PLATE THICKNESS ON THE PLASTIC ZONE REVEALED BY ETCHING THE SURFACES OF MACHINE-NOTCHED Fe-3Si STEEL COUPONS (800°C ANNEAL):

(a)(b) 0.017-inch thick, c/t = 14.7
(c)(d)(e) 0.068-inch thick, c/t = 4.4
(f)(g)(h)&(i) 0.200-inch thick, c/t = 1.3

Morris reagent, oblique lighting, magnification 63X

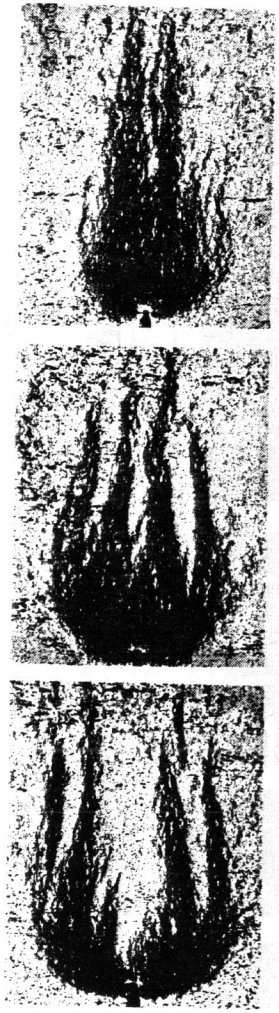

(a) (b) (c)

FIGURE 3. PLASTIC ZONE REVEALED BY ETCHING SECTIONS PARALLEL TO THE TEST COUPON SURFACE

(Fe-3Si, machine notched, 800°C anneal, 0.232-inch thick, $T/Y = 0.9$):
(a) Surface
(b) Section halfway between surface and midsection
(c) Midsection
Morris reagent, magnification **4.29X**

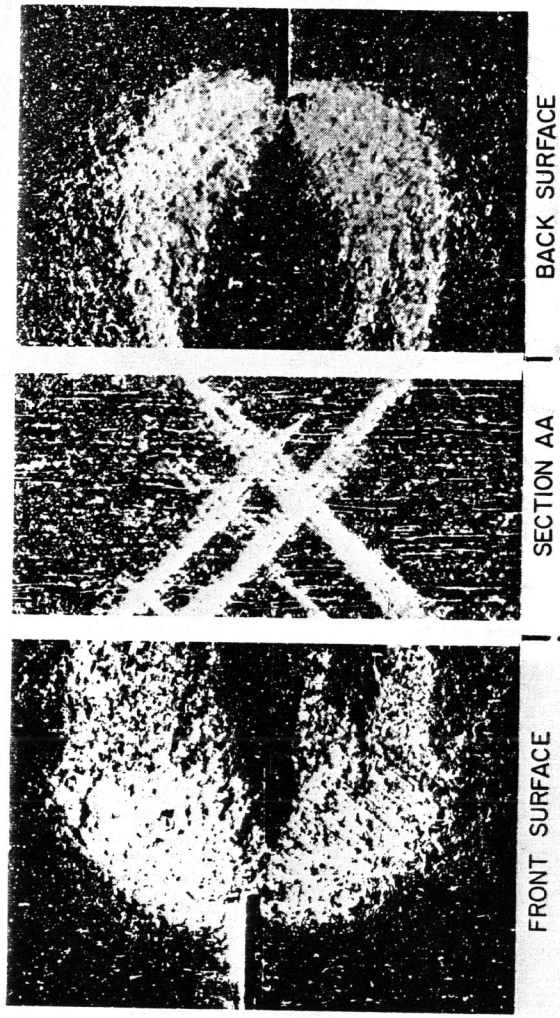

FIGURE 4. APPEARANCE OF PLASTIC ZONE ON THE FRONT SURFACE, BACK SURFACE, AND A NORMAL SECTION

(Fe-3Si, machine notched, 800°C anneal, 0.197-inch thick, $T/Y = 0.9$)
Morris reagent, oblique lighting, magnification **7.93X**

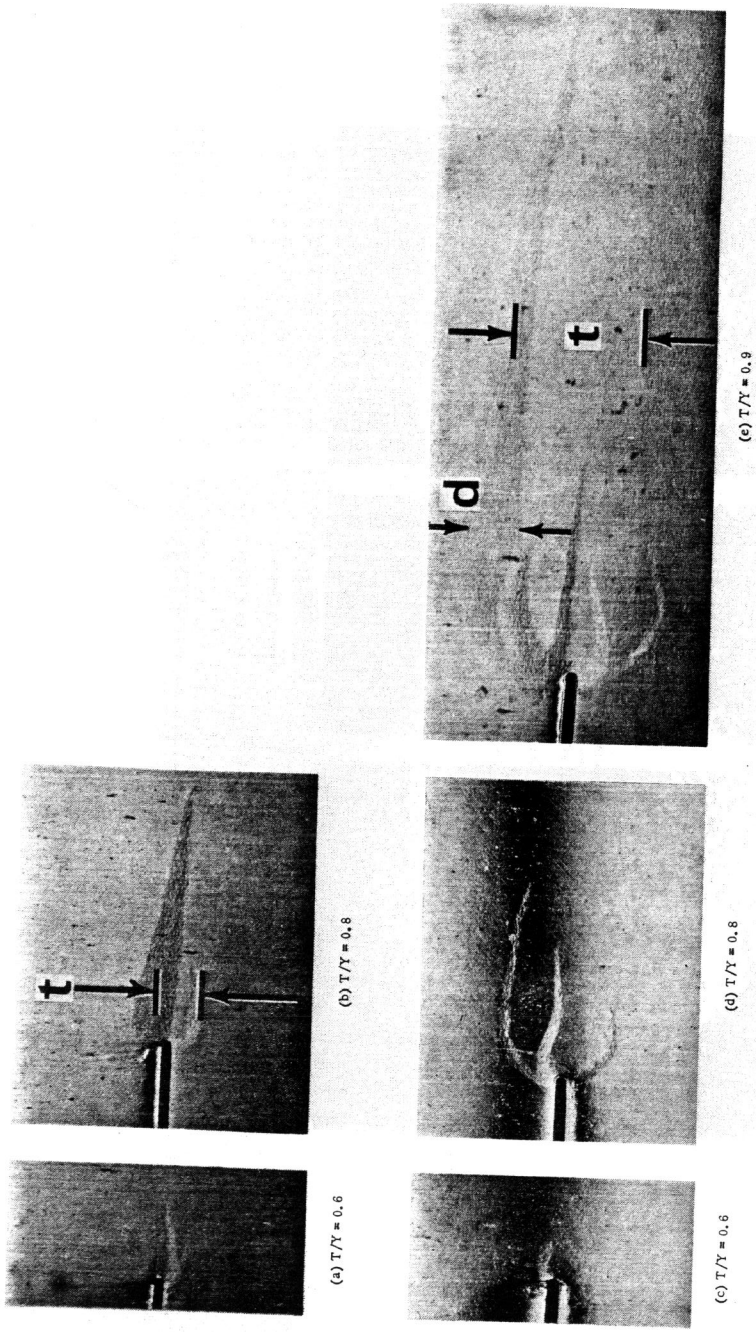

FIGURE 5. INFLUENCE OF NOMINAL STRESS AND PLATE THICKNESS ON THE PLASTIC ZONE REVEALED ON THE SURFACES OF MACHINE-NOTCHED PLAIN CARBON STEEL COUPONS:
(a)(b) 0.058-inch thick, c/t = 4.4
(c)(d)&(e) 0.200-inch thick, c/t = 1.3
Slightly oblique lighting, magnification 4.54X

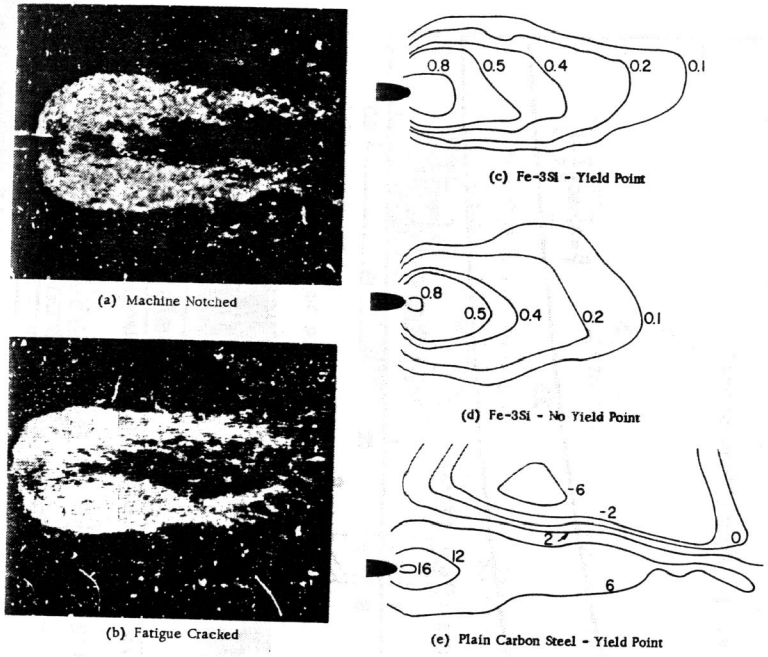

FIGURE 6. PLASTIC ZONES PRODUCED BY LOADING 0.060-INCH-THICK COUPONS TO T/Y = 0.78 AND REVEALED ON THE SURFACE BY ETCHING AND INTERFEROMETRY:
(a) Fe-3Si, machine notched, 800°C anneal (Curve 1.1, Figure 1), etched
(b) Fe-3Si, fatigue cracked, 800°C anneal (Curve 1.1, Figure 1), etched
(c) Same as (a), interferometry
(d) Fe-3Si, machine notched, 1200°C anneal (Curve 1.2, Figure 1), interferometry
(e) Steel E, machine notched (Curve 1.3, Figure 1), interferometry

(a) & (b) Oblique lighting. In (c) & (d), percent strain values are quoted. In (e), the numbers give relative displacements in units of 0.00001 inch. The closely spaced contours -2, 0, +2, +6 are consistent with a 45-degree-inclined wedge-shaped region sheared about 1%.

Magnification 8.54X

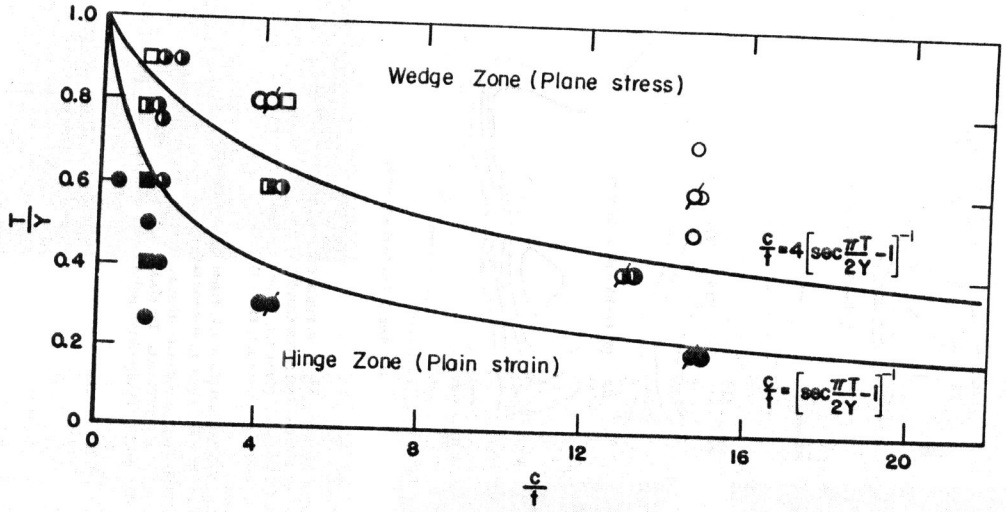

FIGURE 7. INFLUENCE OF STRESS LEVEL, CRACK LENGTH, AND THICKNESS ON THE CHARACTER OF THE PLASTIC ZONE IN Fe-3Si STEEL AND STEEL E

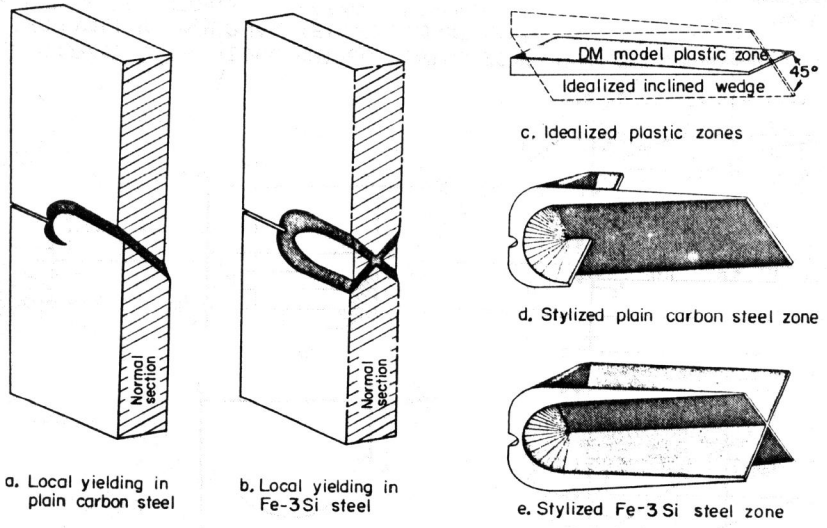

FIGURE 8. THREE-DIMENSIONAL CHARACTER OF PLANE-STRESS PLASTIC ZONES

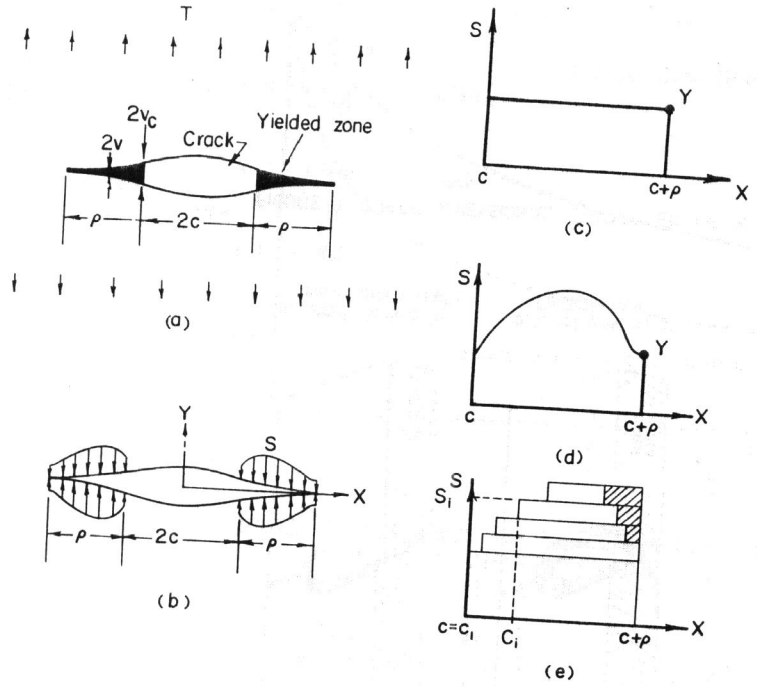

FIGURE 9. THE DM MODEL: (a) CRACK WITH WEDGE-SHAPED PLASTIC ZONES, (b) CRACK WITH "EQUIVALENT" INTERNAL TENSION, (c) UNIFORM TENSION DISTRIBUTION OF DUGDALE, (d) VARYING TENSION DISTRIBUTION, AND (e) STEPWISE APPROXIMATION OF THE VARYING TENSION DISTRIBUTION

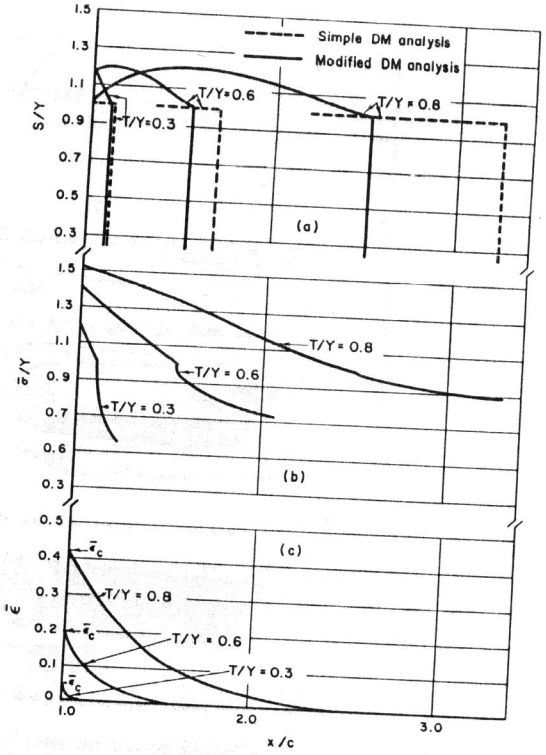

FIGURE 10. STRESS AND STRAIN GRADIENTS CALCULATED FOR A CRACK IN 4330 M STEEL (CURVE 1.4, FIGURE 1c, TABLE 1, c = 3.75 in., t = 0.140 in.):
(a) Internal tension
(b) Stress
(c) True strain (plastic)

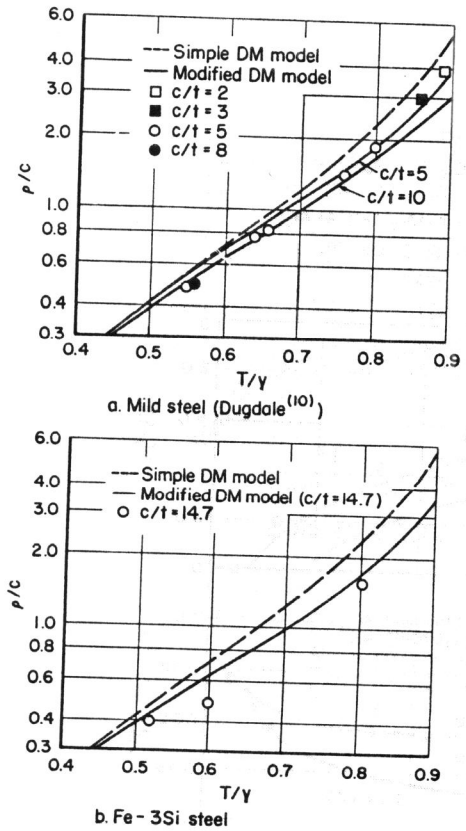

FIGURE 11. COMPARISON OF THE MEASURED AND CALCULATED PLASTIC-ZONE SIZES

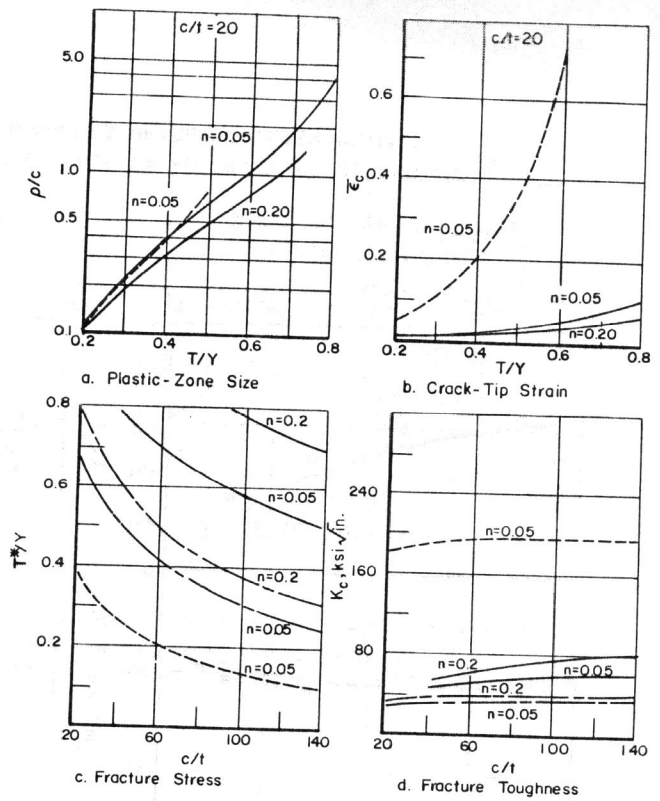

FIGURE 12 INFLUENCE OF STRENGTH LEVEL, WORK HARDENING, AND DUCTILITY AS SHOWN BY CALCULATIONS FOR THE HYPOTHETICAL STEELS OF FIGURE 1c (CURVES 1.7, 1.8, AND 1.9, AND TABLE 1)

—— Y= 30,000 psi, $\bar{\epsilon}^*$=0.4 ------- Y= 300,000 psi, $\bar{\epsilon}^*$=0.4
—·— Y= 30,000 psi, $\bar{\epsilon}^*$=0.1

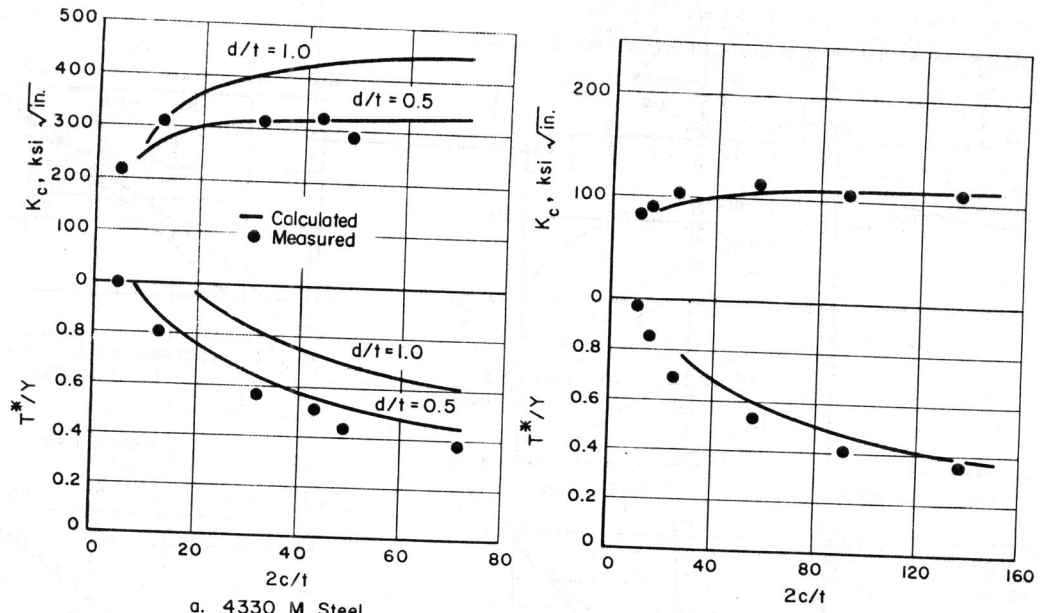

a. 4330 M Steel
(Curve 1.4, Figure 1b, Table 1)

b. 2219-T87 Aluminum
(Curve 1.5, Figure 1b, Table 1)

FIGURE 13. COMPARISON OF CALCULATED FRACTURE STRESS AND K_c LEVELS WITH VALUES MEASURED EXPERIMENTALLY

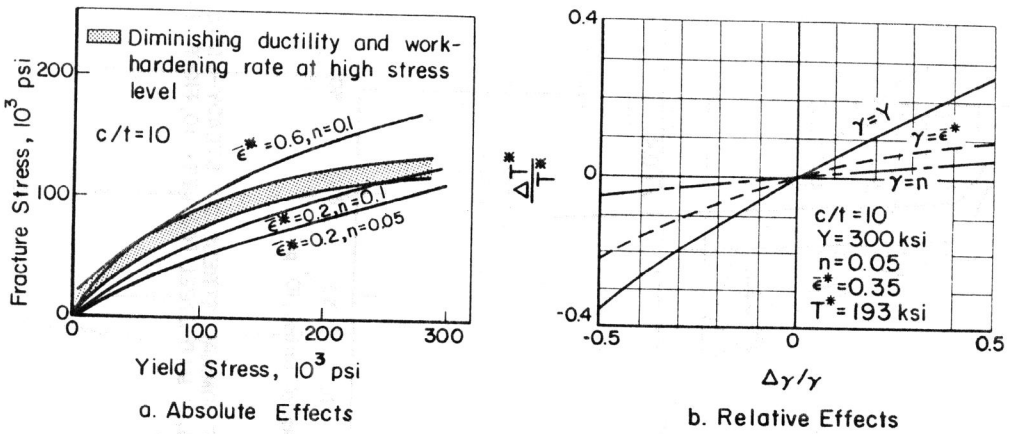

a. Absolute Effects

b. Relative Effects

FIGURE 14. CALCULATED CURVES SHOWING THE INFLUENCE OF YIELD-STRENGTH LEVEL, WORK-HARDENING RATE, AND DUCTILITY ON THE FRACTURE STRESS OF HYPOTHETICAL STEELS (EQUATION 1, TABLE 1)

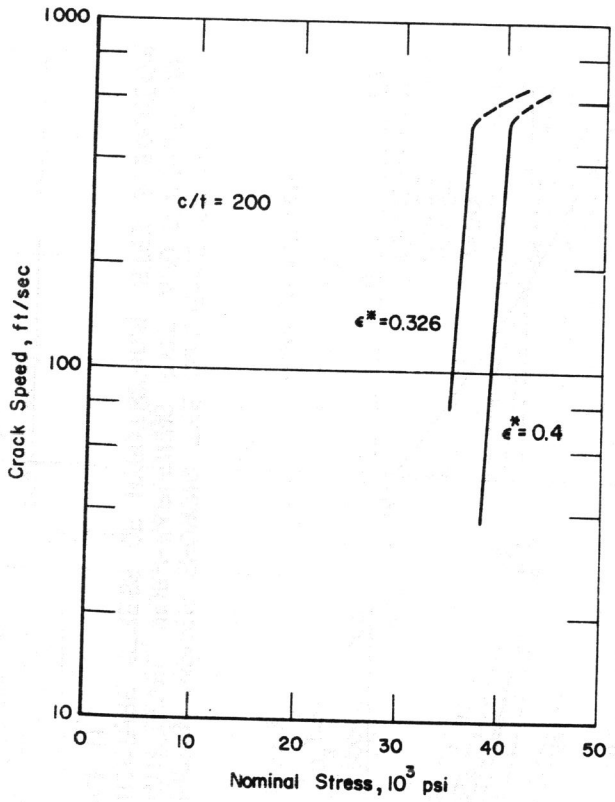

FIGURE 15. INFLUENCE OF NOMINAL STRESS ON STEADY-STATE CRACK SPEED IN MILD STEEL (CURVES 1.10, FIGURE 1d AND TABLE 1)

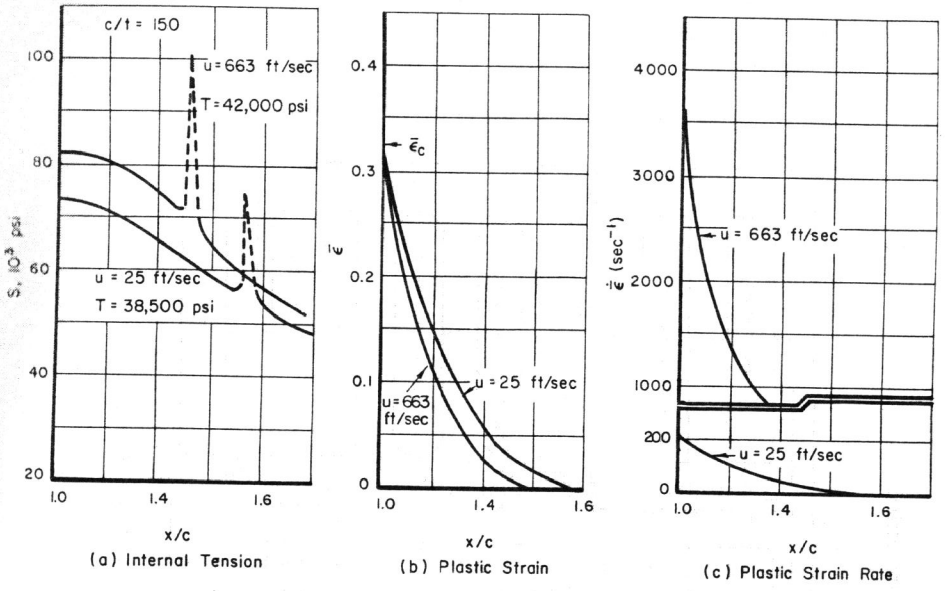

FIGURE 16. TENSION, STRAIN, AND STRAIN RATE IN ADVANCE OF A PROPAGATING CRACK IN MILD STEEL (CURVES 1.10, FIGURE 1d, TABLE 1)

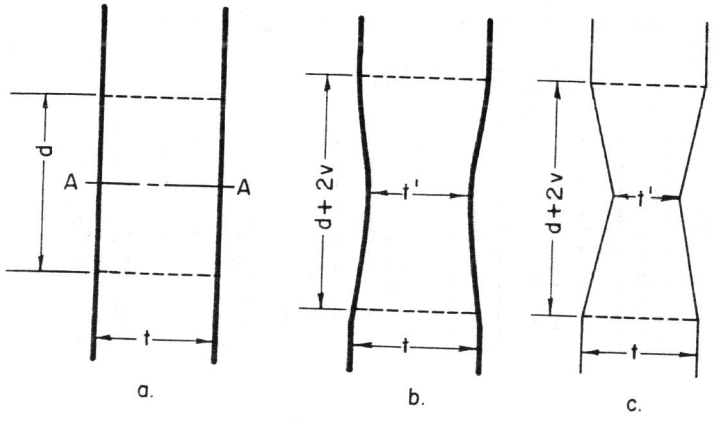

FIGURE B-1. GEOMETRY USED FOR CALCULATING THE DISPLACEMENT-STRAIN RELATION

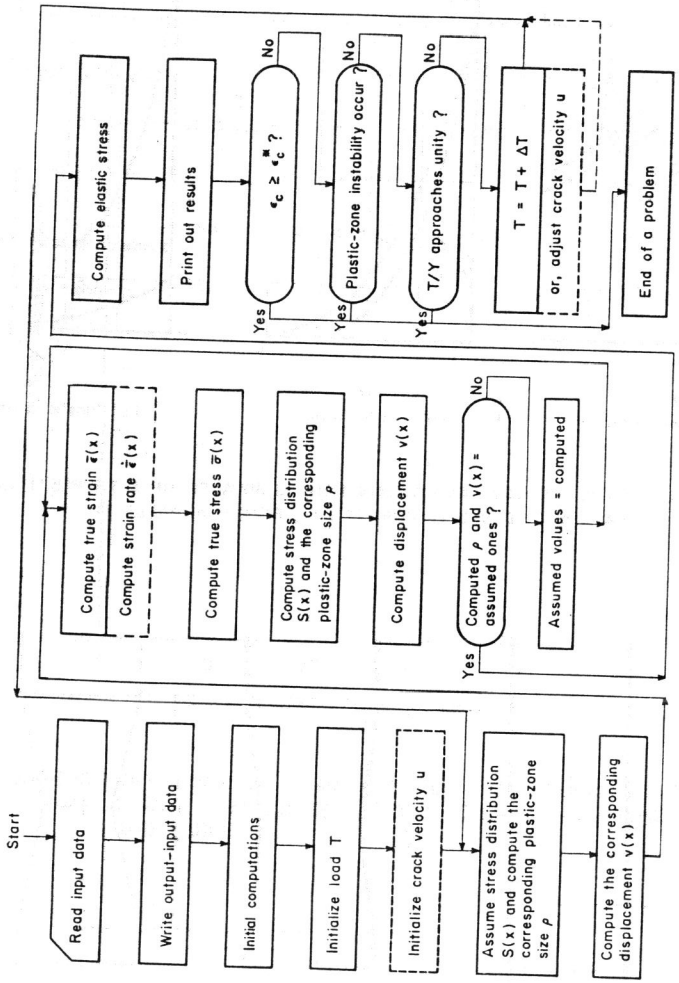

FIGURE C-1. FLOW CHART OF THE COMPUTER PROGRAM

A-16 ELASTO-PLASTIC STRESSES AND STRAINS IN CRACKED PLATES

J.L. Swedlow+*, M.L. Williams+** and W.H. Yang+***

ABSTRACT

A numerical method for analyzing the stresses and strains in work-hardening plates is applied to three crack problems. The first problem is that of an internally cracked plate, the second allows for reduced work-hardening, and the third involves external cracks. Selected data are presented and discussed briefly. One important result indicates that, compared to the elastic solution, the singularity of stress at the crack point decreases with load, while that for strain increases. Also, there are significant differences between internally and externally cracked plates in terms of the stress and strain fields.

+ Firestone Flight Sciences Laboratory, Graduate Aeronautical Laboratories, California Institute of Technology, Pasadena, California U.S.A.
* Research Fellow
** Professor of Aeronautics; presently Professor of Engineering, University of Utah, Salt Lake City, Utah
*** Research Fellow; presently Assistant Professor of Engineering Mechanics, University of Michigan, Ann Arbor, Michigan